a

HoloE (5 mM Ca^{2+})

HoloE (5 mM Mg^{2+})

HoloES (pre-tRNA) (1 mM Ca^{2+})

HoloES (pre-tRNA) (5 mM Ca^{2+})

HoloES (nc-pre-tRNA) (5 mM Ca^{2+})

HoloES (LB-pre-tRNA tilt1) (5 mM Ca^{2+})

HoloES (LB-pre-tRNA tilt2) (5 mM Ca^{2+})

HoloEP (mat-tRNA) (5 mM Ca^{2+})

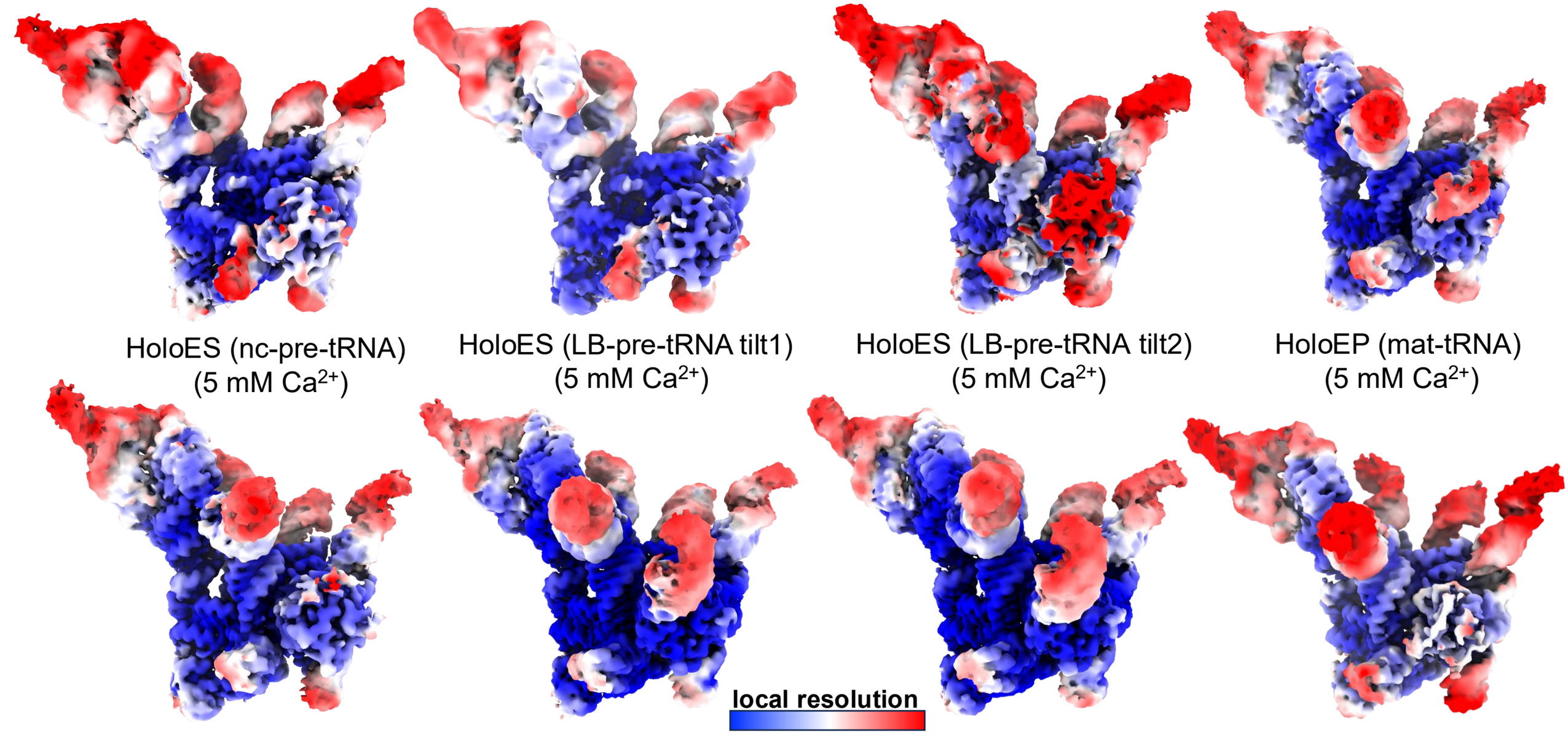

local resolution

2.5 4.0 6.0 (Å)

b

HoloE (5 mM Ca^{2+})

HoloE (5 mM Mg^{2+})

HoloES (pre-tRNA) (1 mM Ca^{2+})

HoloES (pre-tRNA) (5 mM Ca^{2+})

HoloES (nc-pre-tRNA) (5 mM Ca^{2+})

HoloES (LB-pre-tRNA tilt1) (5 mM Ca^{2+})

HoloES (LB-pre-tRNA tilt2) (5 mM Ca^{2+})

HoloEP (mat-tRNA) (5 mM Ca^{2+})

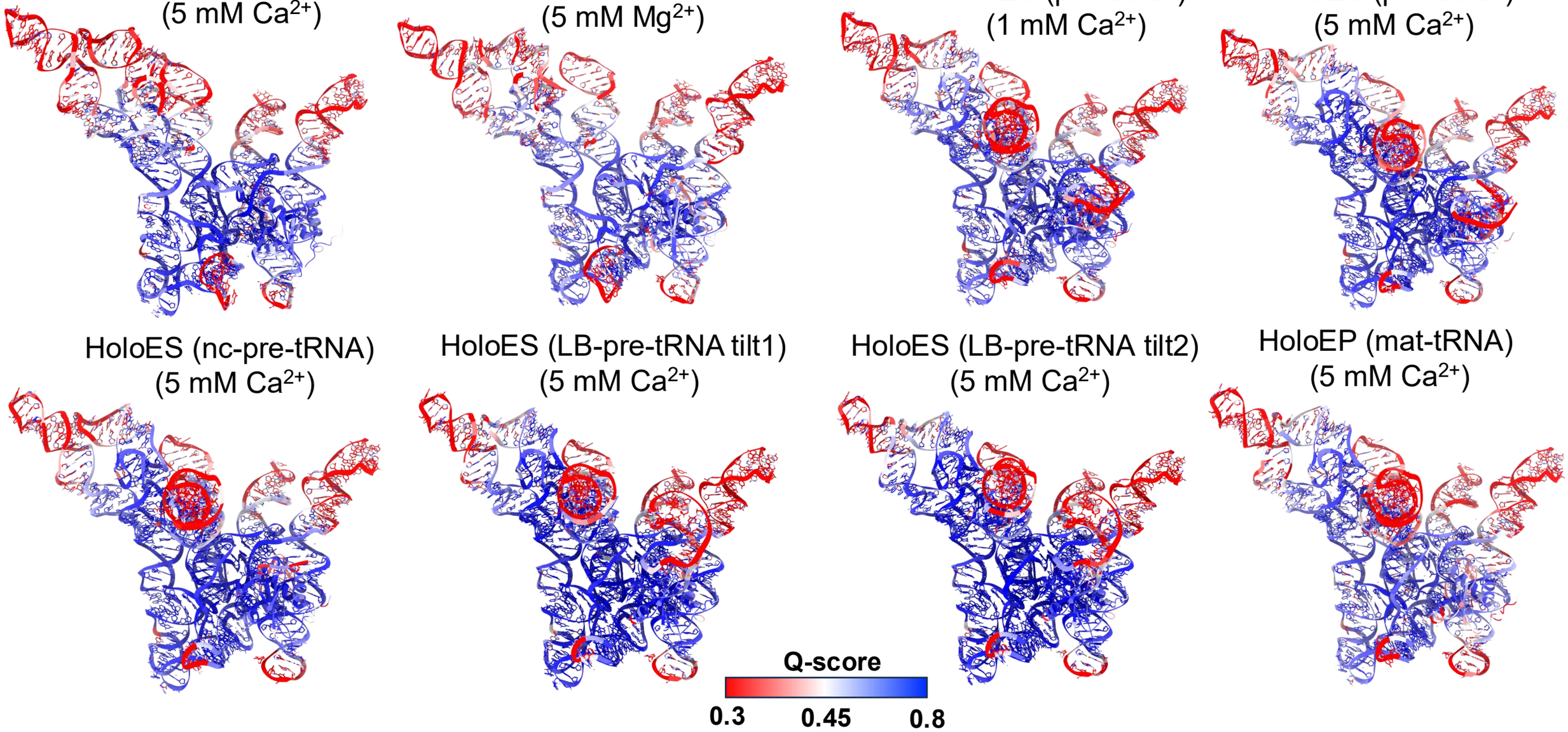

Q-score

0.3 0.45 0.8

Extended Data Fig. 1 | Local structural resolution of cryo-EM volumes and Q-score assessments for corresponding all-atom models. a, Local resolution estimation and **b,** per-nucleotide Q-score mapping of the cryo-EM consensus volumes of the 8 wild-type RNase P holoenzymes in this study. The local resolution and Q-score were mapped on all volumes from blue, white, and red in an ascending and descending manner on the scale bar, respectively.

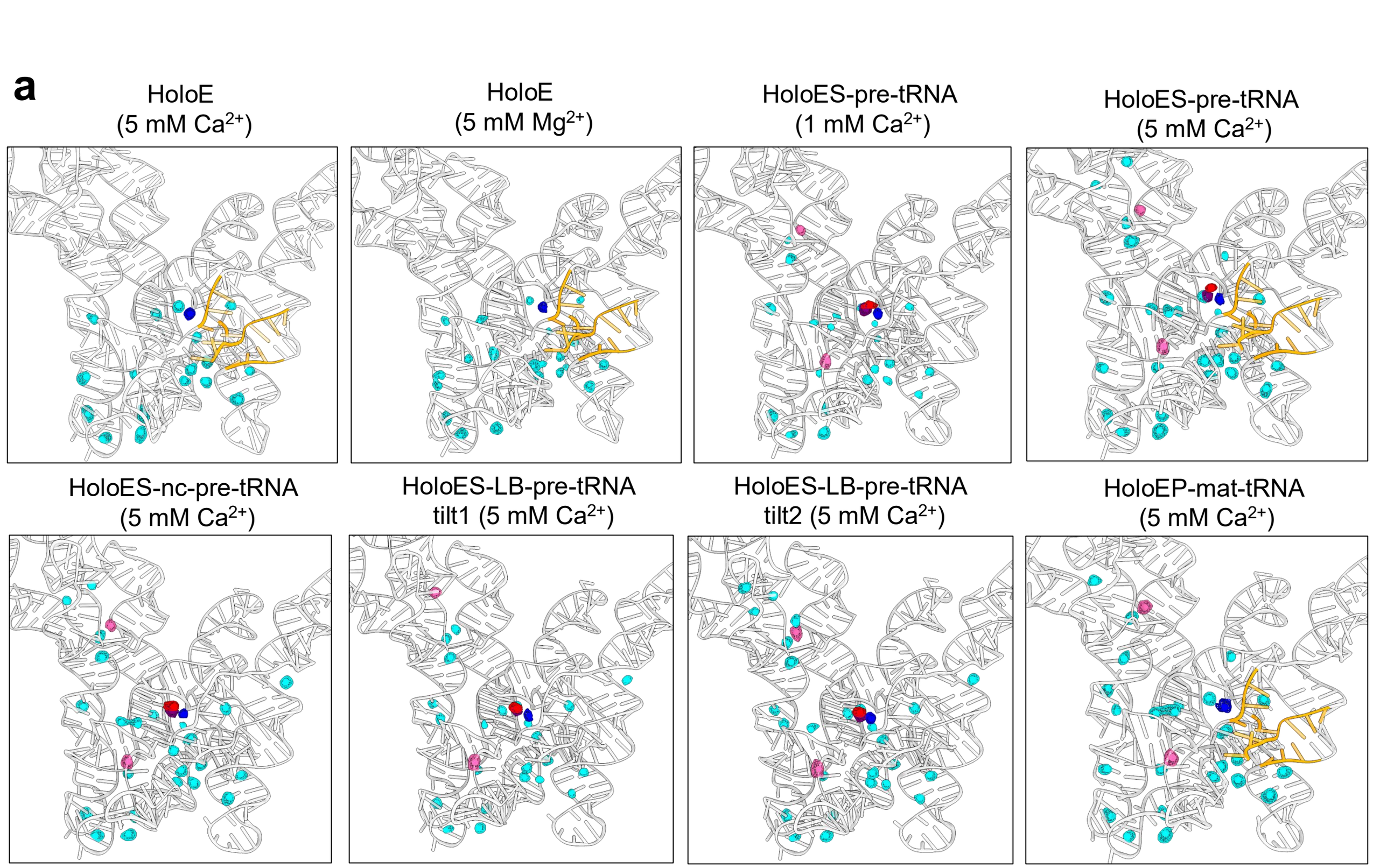

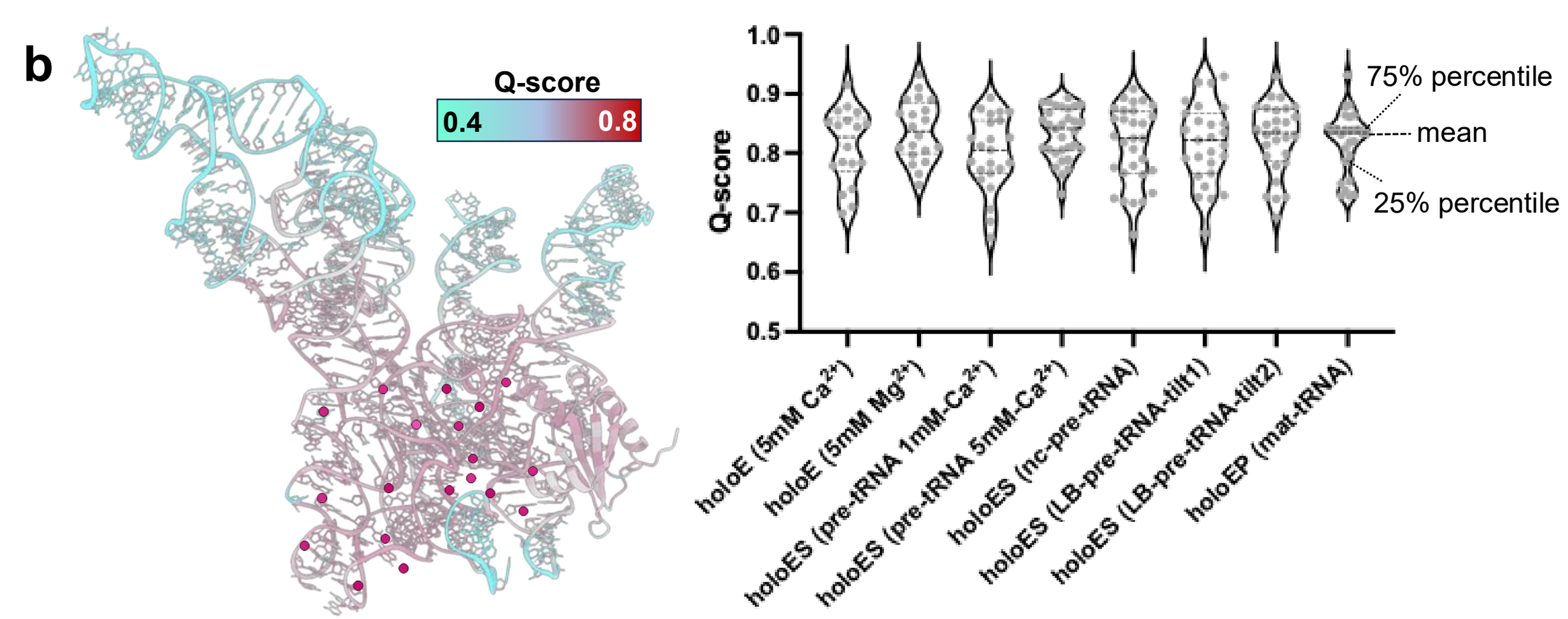

Extended Data Fig. 2 | Divalent metal ion density maps and Q-scores in the cryo-EM structures. a, Divalent metal ions of all the wild-type RNase P holoenzyme structures, and the ions are superimposed with their cryo-EM maps at a contour level threshold of 10 standard deviation (σ). The RNase P protein component, rnpA binding site, is colored in orange. **b,** Q-score assessment and mapping of the metal ions on holoE structure. Statistics of Q-score distribution of all structures displayed in a Violin plot.

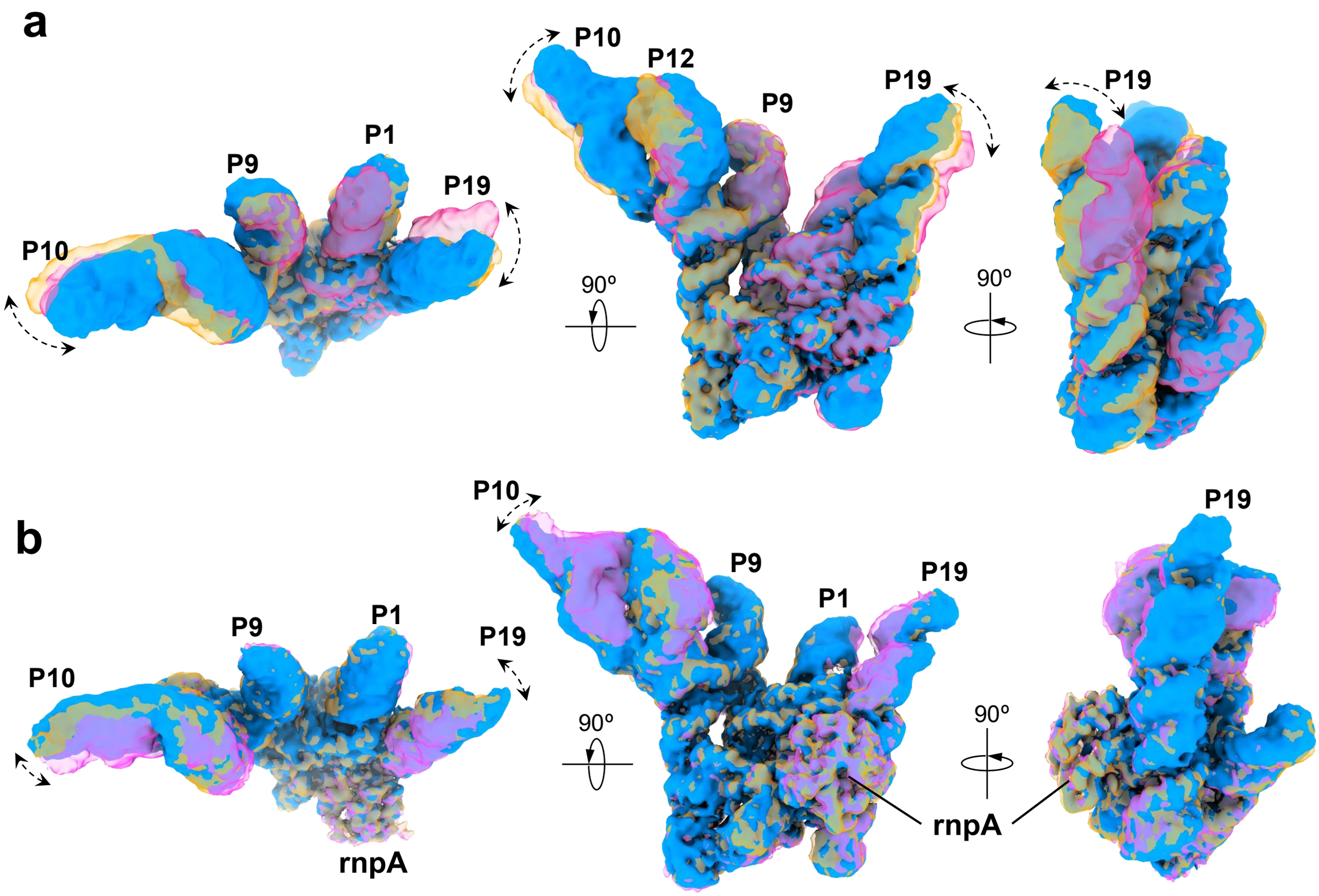

Extended Data Fig. 3 | Structural variability of RNase P apoenzyme (apoE) and holoenzyme (holoE). The three distinct conformations of the **a.,** apoE and **b.,** holoE, with different molecular surface colors, were subclassified and determined using three-dimensional classification in cryoSPARC **(Method).** The two conformations of apoE and holoE (magenta and orange), aligned against the structure, generated from the majority of particles (blue).

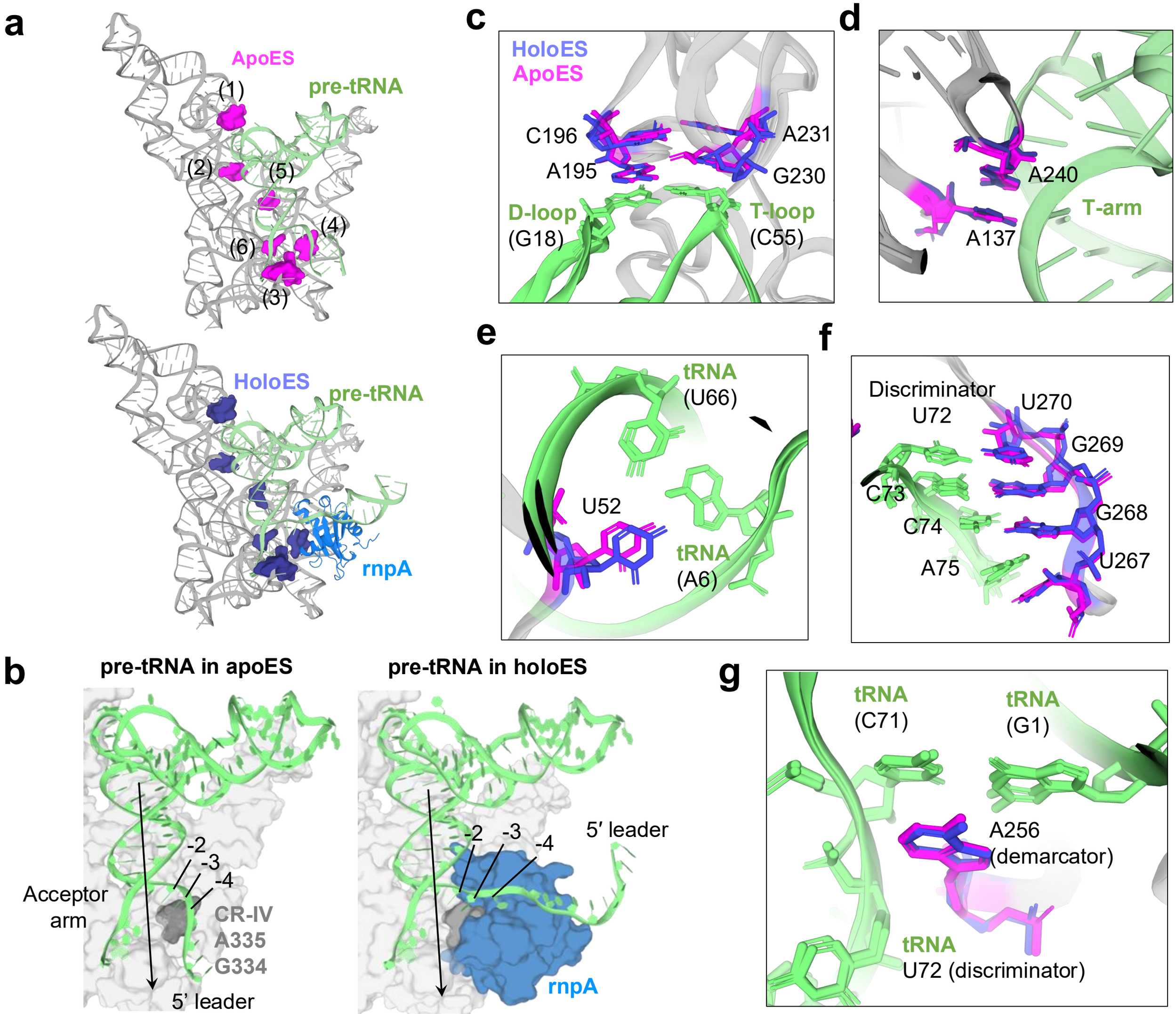

Extended Data Fig. 4 | Local structural comparison of the six toeholds for pre-tRNA recognition between RNase P apo and holoenzymes. a, Structures of apoES (top) and holoES (bottom) with the five toeholds shown with the molecular surface, colored with magenta and blue, respectively. **b,** 5′ leader interactions in apoES and holoES. **c,** Base stacking interaction between RNase P RNA (RPR) IDTM and tRNA elbow region. **d,** RPR bulge interactions (A137 and A240) with the minor groove of the T arm of pre-tRNA. **e,** RPR U52 forms a base triplet with an AU base pair in the tRNA acceptor arm. **f,** RPR L15 interaction with the 3′-CCA trailer of pre-tRNA. **g,** The discriminator and demarcator nucleobases of pre-tRNA and RPR, respectively.

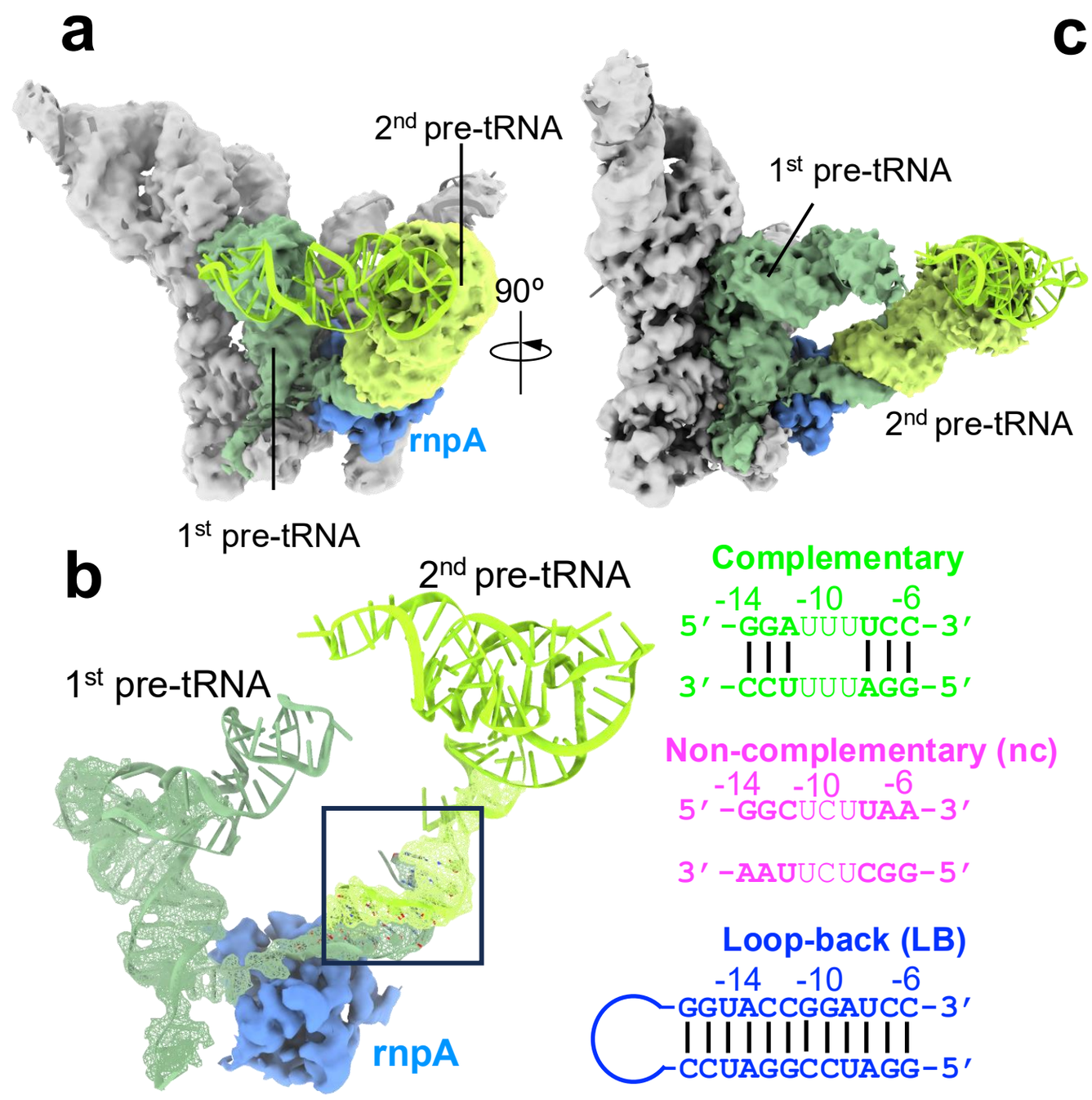

Extended Data Fig. 5 | The presence of the second pre-tRNA in RNase P holoES. a, In holoES, the pre-tRNA 5′-leader conformation promotes annealing with a second pre-tRNA molecule through sequence complementarity in the region upstream (-14 to -6) that extends beyond the RPR-tRNA interface. **b,** Two pre-tRNA models annealed by the 5'-leader sequence complementarity. Cognate pre-tRNA binding interface in holoES and designs of non-complementary (nc) and loop-back (LB) pre-tRNA variants for preventing pre-tRNA dimer annealing *via* 5′ leader. **c,** HoloES structures show similar interactions with the 5′ leader of pre-tRNA variants (nc- and LB-pre-tRNA) up to C-5**.**

a

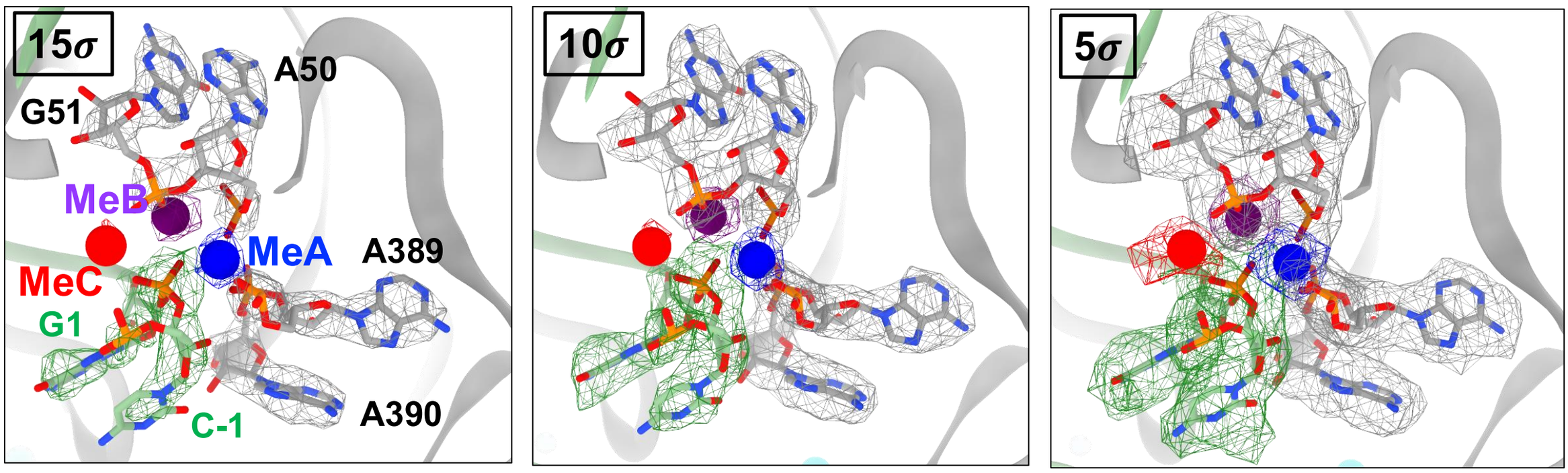

b

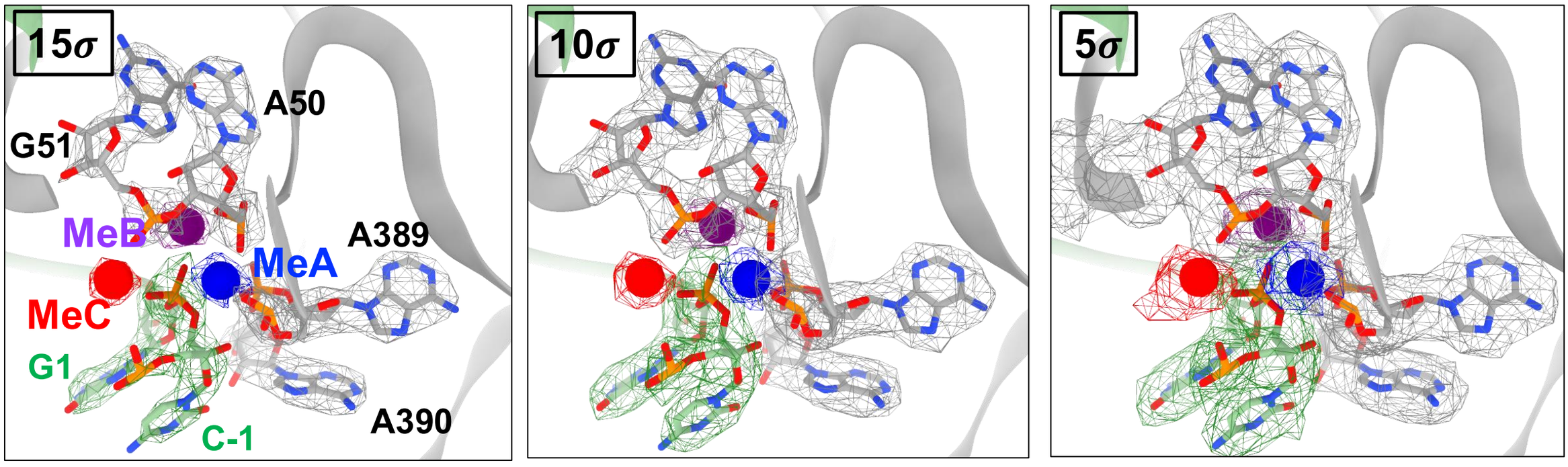

Extended Data Fig. 6 | The catalytic metal ions in RNase P holoES complexes determined at 1 and 5 mM Ca^{2+}. Structures of the catalytic nucleotides and the three divalent metal ions (MeA-C), superimposed with cryo-EM maps with a decreasing contour level threshold (from left to right) that were determined **a,** at a physiologically relevant concentration of 1 mM Ca^{2+} and **b,** at an elevated concentration of 5 mM Ca^{2+}.

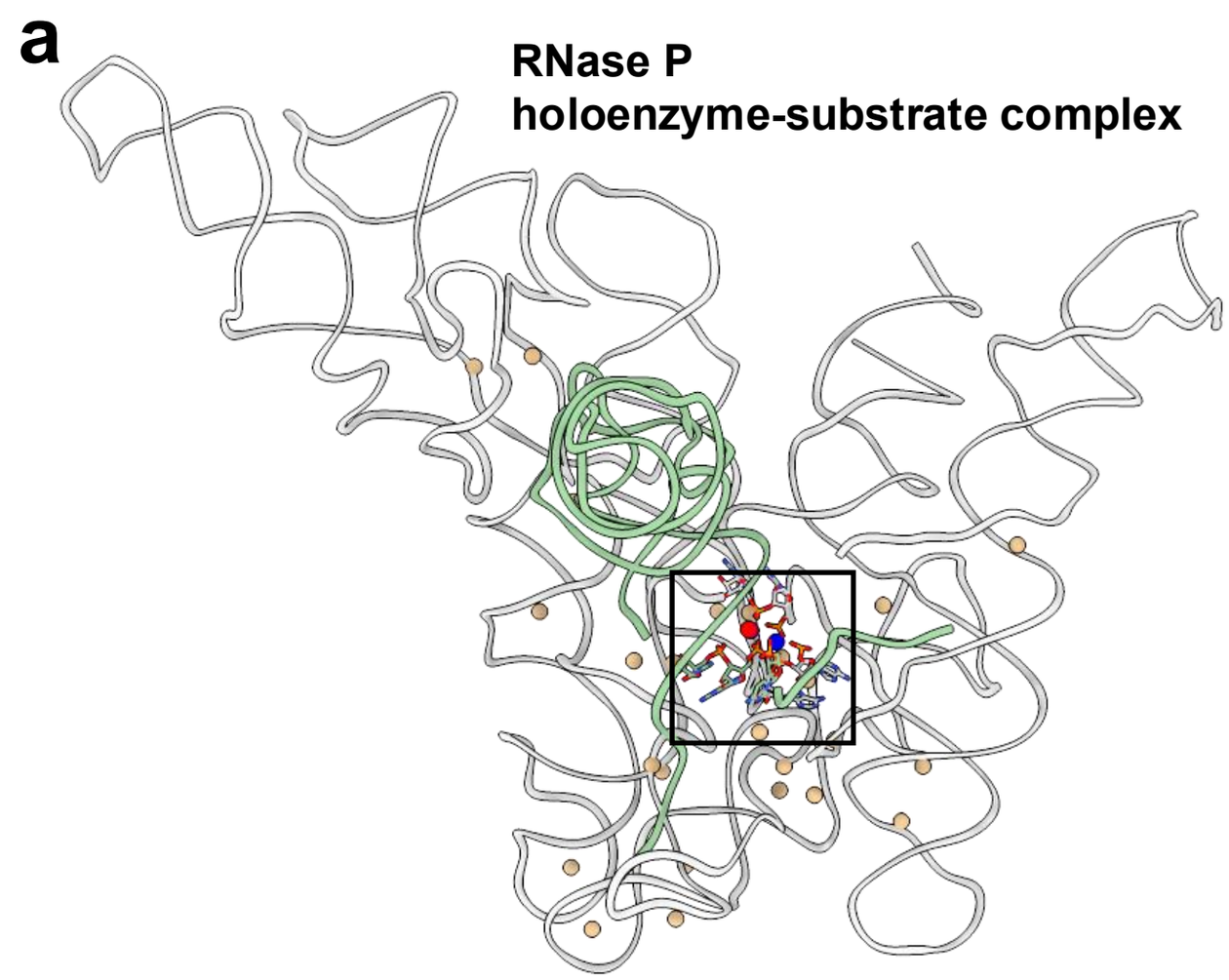

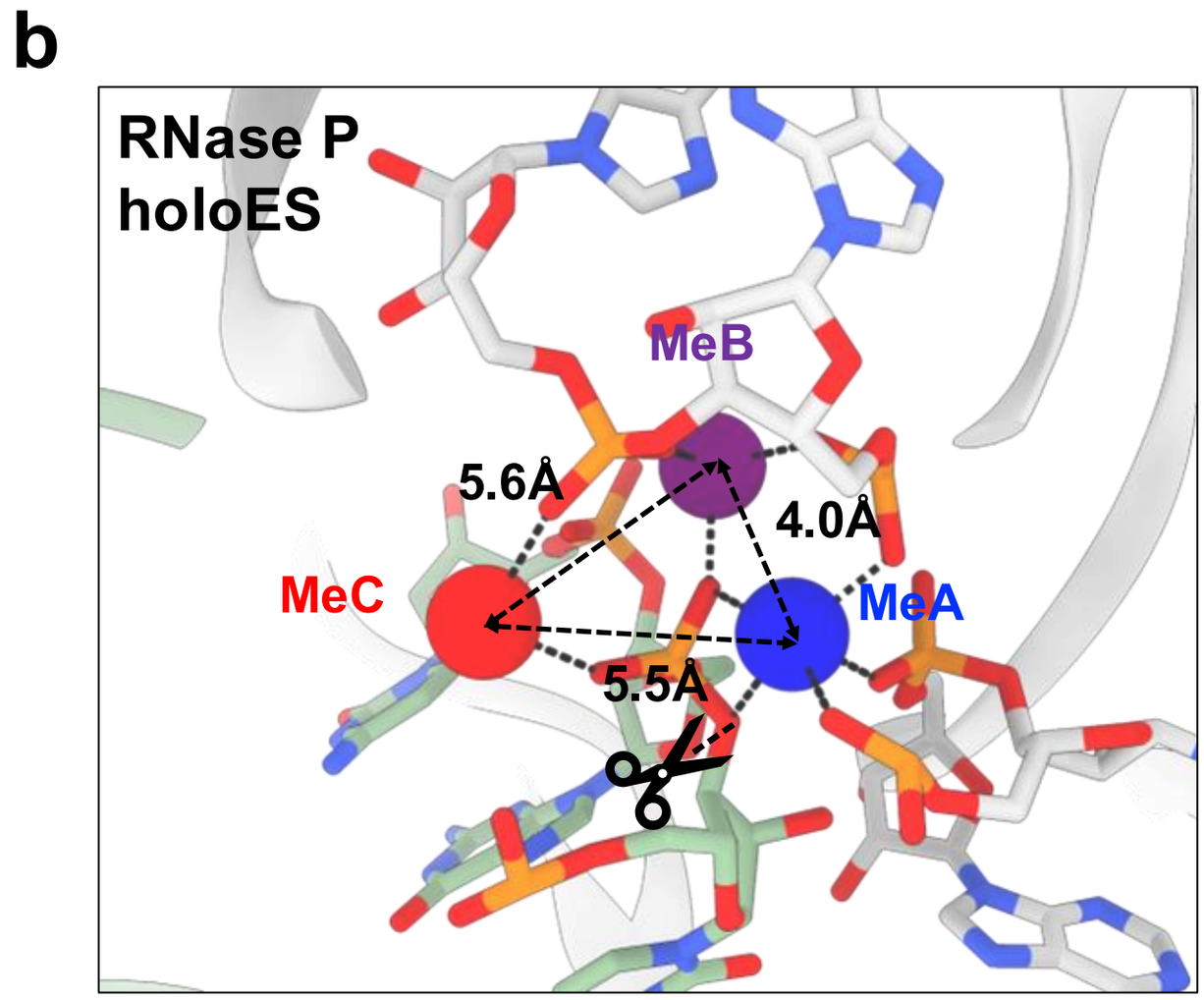

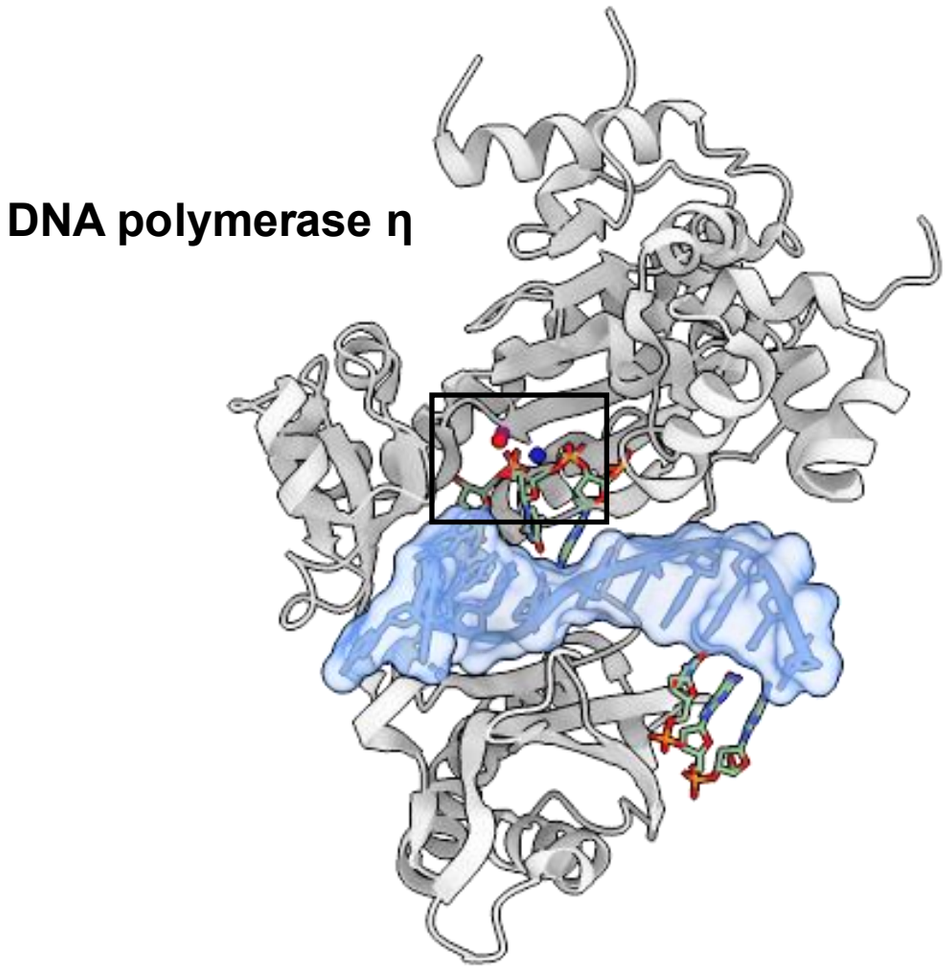

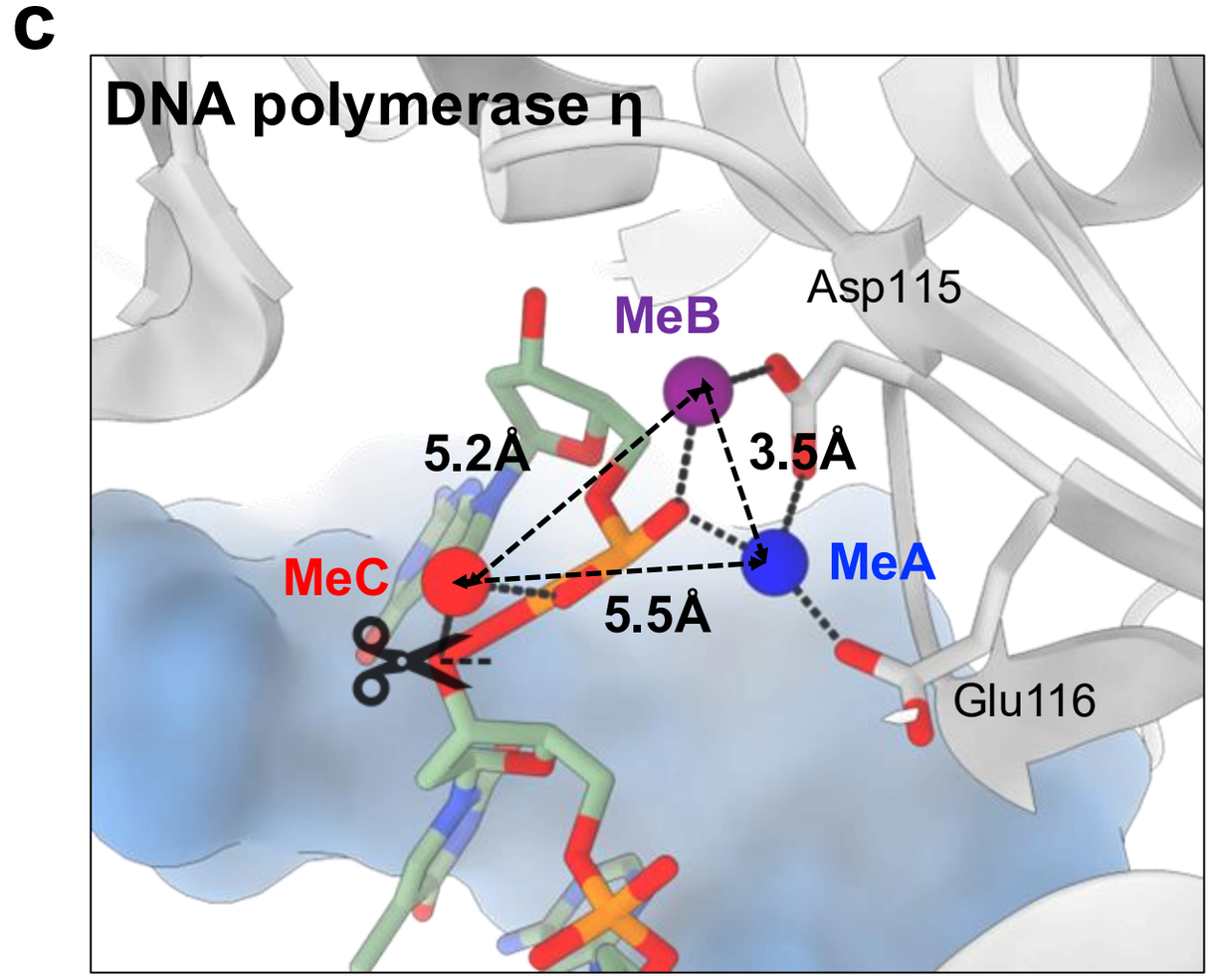

Extended Data Fig. 7 | Catalytic metal ion triad in RNase P holoenzyme and human DNA polymerase η | a, Structures of RNase P holoenzyme-pre-tRNA substrate complex (PDB: 9OWT in this study) and human DNA polymerase η in complex with double-stranded DNA (PDB: 7U79). The catalytic metal ion triad in **b,** RNase P-substrate complex and **c,** human DNA polymerase are highlighted and zoomed out on the right two panels.

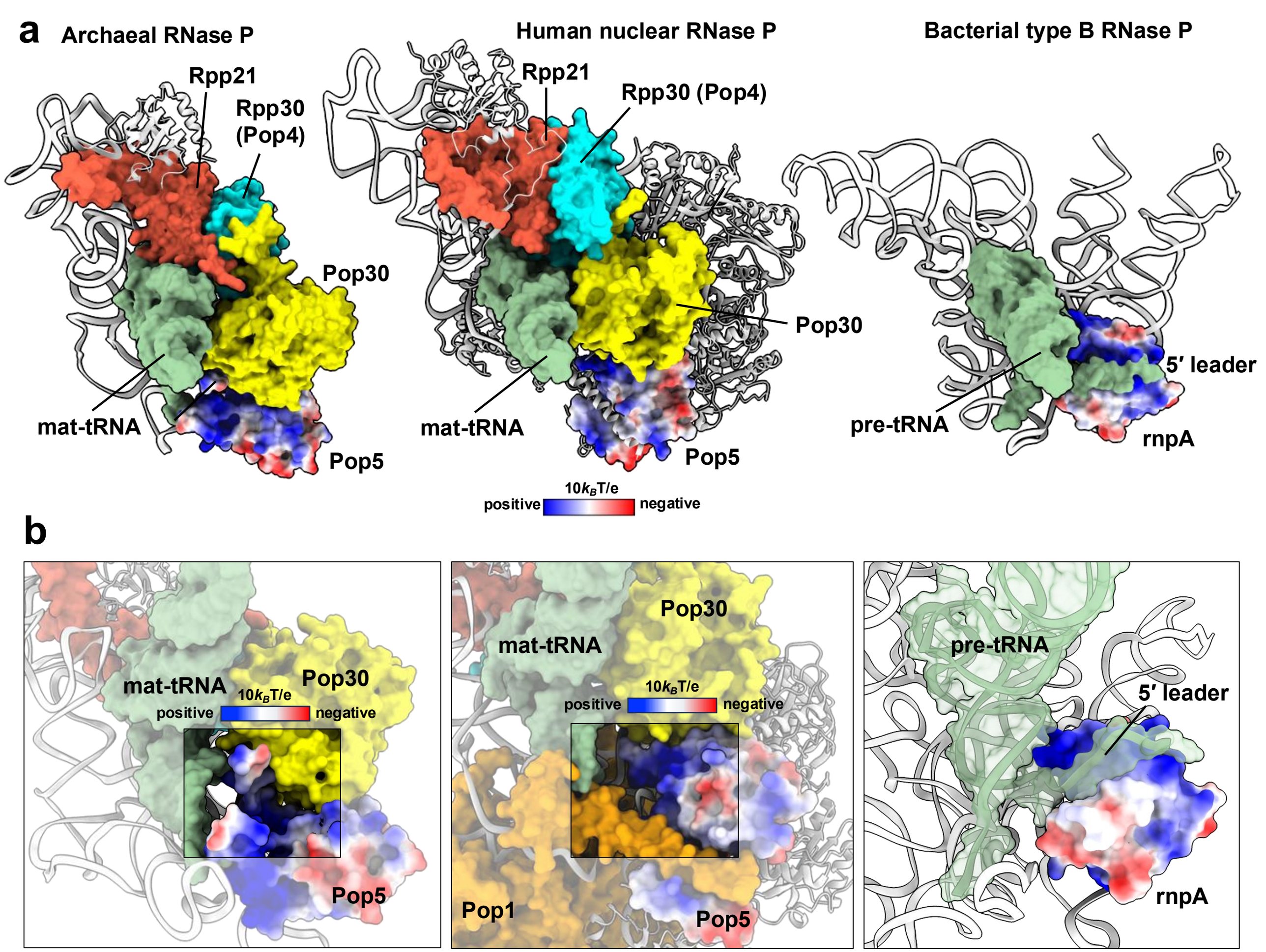

Extended Data Fig. 8 | Comparative structural analysis for archaeal, human nuclear and bacterial RNase Ps. a, RNase P structures of archaeal, human nuclear and bacterial RNase Ps (PDBs: 6K0B, 6AHU, 9OWT from left to right). The protein components of the archaeal, human nuclear RNase Ps showed in molecular surface with distinct colors. **b,** The protein component Pop5 in archaeal RNase P (left) , human nuclear RNase P (middle) and rnpA of bacterial RNase P (far-right) are coloring with a color-ramp surface by the values of the electrostatic potential.